Bifurcation structure of a swept-source laser

A. V. Kovalev,[1,*] P. S. Dmitriev,[1] A. G. Vladimirov,[2] A. Pimenov,[2] G. Huyet,[3] and E. A. Viktorov[1]
[1]*ITMO University, Birzhevaya Liniya 14, 199034 Saint Petersburg, Russia*
[2]*Weierstrass Institute for Applied Analysis and Stochastics, Mohrenstrasse 39, D-10117 Berlin, Germany*
[3]*Université Côte d'Azur, Centre National de La Recherche Scientifique, Institut de Physique de Nice, F-06560 Valbonne, France*

(Received 7 August 2019; published 21 January 2020)

We numerically analyze a delay differential equation model of a short-cavity semiconductor laser with an intracavity frequency-swept filter and reveal a complex bifurcation structure responsible for the asymmetry of the output characteristics of this laser. We show that depending on the direction of the frequency sweep of a narrow-band filter, there exist two bursting cycles determined by different parts of a continuous-wave solutions branch.

DOI: 10.1103/PhysRevE.101.012212

I. INTRODUCTION

Optical coherence tomography (OCT) has enabled the fast and reliable visualization of various tissues for medical assessment [1]. Swept-source OCT is a technology that relies on coherent lasers that can scan hundreds of nanometers in a few microseconds to enable real-time videos and, as a result, has found a wide range of medical applications in areas such as ophthalmology and cardiology [2]. To obtain such performance, researchers have developed novel frequency-swept light sources, such as Fourier domain mode-locked lasers (FDMLs) [3], short external cavity lasers [4–7], vertical cavity surface-emitting lasers (VCSELs) with microelectromechanical system (MEMS) driven filters [8–11], multisection semiconductor lasers [12], and photonic integrated circuit devices [13]. The underlying operation principle of these devices relies on laser cavities incorporating a broad-band gain medium and a fast tuning mechanism. Semiconductor quantum well active media can be engineered to deliver broadband gain amplification; however, the development of a fast tuning mechanism is a challenge because it may degrade the laser emission. FDMLs have a kilometer-long ring cavity containing an intracavity filter that is driven in resonance with the round-trip time. At the other extreme, VCSELs have a cavity length of a single optical wavelength, and their tunability is achieved by a slight modification of the cavity length.

Nonlinear dynamical regimes in FDML devices can be theoretically modeled by partial differential equations governing the spatiotemporal evolution of the complex envelope of the electric field [14,15]. Another powerful method to describe these lasers is based on the use of delay differential equations (DDEs) [16,17]. In particular, the experimentally observed asymmetry in the output dynamics between the filter sweeping from shorter to longer wavelengths and the filter sweeping from longer to shorter wavelengths has been successfully explained using the DDE FDML model [16]. It was shown that instabilities observed in FDMLs can be related to short- and long-wavelength modulation instabilities commonly found in nonlinear spatially distributed systems. The same model was able to describe the appearance of the so-called "sliding frequency mode locking" in short-cavity frequency swept lasers [18]. Shorter cavity length devices are appealing as comparably inexpensive and compact swept OCT sources and have recently attracted significant attention [7,11–13]. These lasers, however, demonstrate a wide range of dynamical regimes during the filter sweeping [18] detrimental to the performance of OCT sources, which were observed only in numerical simulations. Therefore, further analysis and understanding of the dynamical properties of such devices is important for the improvement of their characteristics necessary for future applications.

Unlike Ref. [16], where the asymmetry of the FDML was studied in the long-cavity limit, in this paper we consider the case when the cavity length is relatively small and the free spectral range is larger than the bandwidth of the tunable filter. We show that in this case the experimentally observed asymmetry of the laser output with respect to sweep direction is related to the presence of a fold and Andronov-Hopf bifurcations of a very asymmetric branch of continuous wave (CW) regimes. Furthermore, we present a detailed bifurcation analysis of the model equations, discuss coexisting dynamical regimes such as longitudinal mode hopping, quasiperiodic pulsations, and chaos, and compare the results with those obtained earlier [16] for a long-cavity laser.

II. THE MODEL

We consider a DDE model [16] for the normalized complex amplitude of the electrical field $\tilde{E}$ and the time-dependent dimensionless cumulative saturable gain G:

$$\gamma^{-1}\frac{d\tilde{E}}{dt} + (1 + i\Delta)\tilde{E} = \sqrt{\kappa}e^{\frac{1-i\alpha}{2}G}\tilde{E}(t-1), \tag{1}$$

$$\eta^{-1}\frac{dG}{dt} = J - G - (e^{G} - 1)|\tilde{E}(t-1)|^2, \tag{2}$$

where $t \equiv t'/T$, t' is time, and T is equal to the cold cavity round-trip time. The attenuation factor κ describes the total

*avkovalev@niuitmo.ru

nonresonant linear intensity losses per cavity round trip, α is the line-width enhancement factor in the gain, and γ is the bandwidth of the intracavity spectral filtering multiplied by the round-trip time T. $\gamma < 1$ ($\gg 1$) corresponds to the short (long) cavity. J is the pump parameter, and $\eta = O(1)$ is the ratio of the cold cavity round-trip time and the carrier density relaxation time. The time-dependent parameter $\Delta = \Delta(t)$ defines the detuning between the central frequency of the narrow-band tunable filter and the reference frequency, which coincides with the frequency of one of the laser modes. After the coordinate change $\tilde{E} = Ee^{-i\int_0^t \Delta(x)\,dx}$, Eqs. (1)–(2) are transformed into

$$\gamma^{-1}\frac{dE}{dt} + E = \sqrt{\kappa}e^{\frac{1-i\alpha}{2}G - i\phi(t)}E(t-1), \tag{3}$$

$$\eta^{-1}\frac{dG}{dt} = J - G - (e^G - 1)|E(t-1)|^2, \tag{4}$$

where $\phi(t) = -i\int_{t-1}^{t}\Delta(x)\,dx$. Note that Eqs. (3)–(4) are invariant with respect to the shifts $\phi \to \phi + 2\pi n$, where $n = 0, \pm 1, \pm 2, \ldots$, is an integer number. Therefore, all bifurcation diagrams studied here are 2π-periodic on ϕ.

We first consider Eqs. (3)–(4) for the static $\phi(t) = \phi_0$ and define the CW cavity mode solution as $E = \sqrt{I_s}e^{i\omega t}$ with time-independent intensity I_s and the constant gain $G = g$. Different CW solutions correspond to different longitudinal modes of the laser. The relation between the field intensity I_s and the value of the saturable gain g is given by

$$I_s = \frac{J - g}{e^g - 1}. \tag{5}$$

By solving this equation with respect to the gain, $g = g(I_s)$, we obtain two values of the modal frequency corresponding to a given value of the intensity I_s:

$$\omega = \pm\gamma[\kappa e^{g(I_s)} - 1]. \tag{6}$$

Finally, substituting Eq. (6) into the transcendental equation

$$\phi_0 = -\omega - \frac{\alpha g(I_s)}{2} - \arctan\left(\frac{\omega}{\gamma}\right) + 2\pi n, \tag{7}$$

with $n = 0, \pm 1, \pm 2, \ldots$, we get an implicit equation relating the intensity I_s and the parameter ϕ_0. The branch of CW solutions defined by Eqs. (5)–(7) with $n = 0$ is shown in Fig. 1 for the case of a long-cavity (a) and short-cavity (b) laser. All other CW branches can be obtained by a shift $\phi_0 \to \phi_0 + 2\pi n$ with integer n. It is seen that in a long-cavity laser studied in Ref. [16], the CW branch is almost symmetric with respect to the reflection $\phi_0 \to -\phi_0$.

In a short-cavity laser, the CW branch can be very asymmetric with a foldover, which is generally characteristic for nonlinear resonators [19,20]. The fold bifurcation points in the Fig. 1(b), corresponding to the extrema of the function $\phi_0(\omega)$ defined by (7), can be found by solving $d\phi_0/d\omega = 0$ and read

$$\omega_{LP} = [-\alpha \pm \sqrt{\alpha^2 - 4\gamma(\gamma+1)}]/2. \tag{8}$$

Inequality $\alpha^2 > 4\gamma(1+\gamma)$ defines the condition for appearance of the foldover. One of the two fold points defined by (8) corresponds to the small intensity and another to the large intensity, as can be seen in Fig. 1(b). The latter fold bifurcation

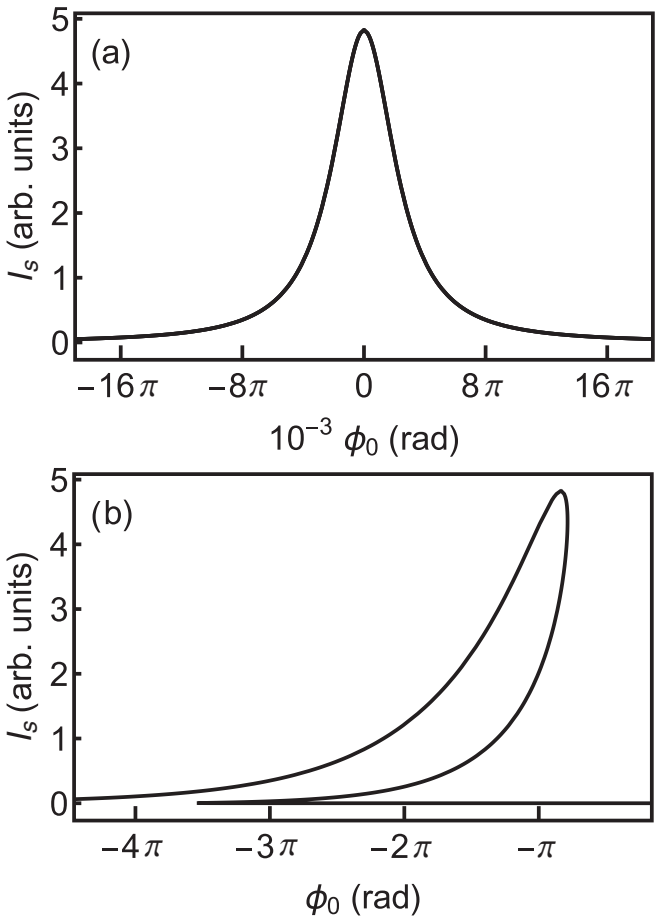

FIG. 1. Branch of CW solutions in a long-cavity (a) ($\gamma = 100$) and short-cavity (b) ($\gamma = 0.25$) laser. Other parameter values are $J = 10$, $\kappa = 0.35$, and $\alpha = 5$.

is responsible for the stability loss of a CW regime in a laser with adiabatically slowly increasing ϕ_0.

III. SWEEPING DYNAMICS

Let us now explore the effect of a slowly varying $\phi(t) = \pm\varepsilon t$, $\varepsilon \ll 1$, which corresponds to the frequency sweep in opposite directions with a sweeping rate which is much slower than one wavelength per round trip. Time trace in Fig. 2 results from direct numerical integration of Eqs. (3)–(4), and demonstrates well-known asymmetry of the dynamical response to the frequency sweep. The bifurcation diagram of the steady and periodic solutions in Fig. 3 has been computed using a numerical continuation technique [21] and displays the cavity mode branches for $n = 1$ and $n = 2$ in the range $0 < \phi_0 < 4\pi$. Because of the periodicity in ϕ_0, the cavity mode branch for $n = 2$ is the same as the one for $n = 1$ but shifted by 2π along the ϕ_0 axis. The low-amplitude tail of the branch for $n = 2$ overlaps with the large-amplitude part of the branch for $n = 1$. This overlap is important for understanding the two types of the bursting dynamics which appear with frequency sweeping in opposite directions. Each branch contains two important bifurcations marked in Fig. 3 as H and LP, and a stable steady-state laser operation is possible only in the interval between these points. LP corresponds

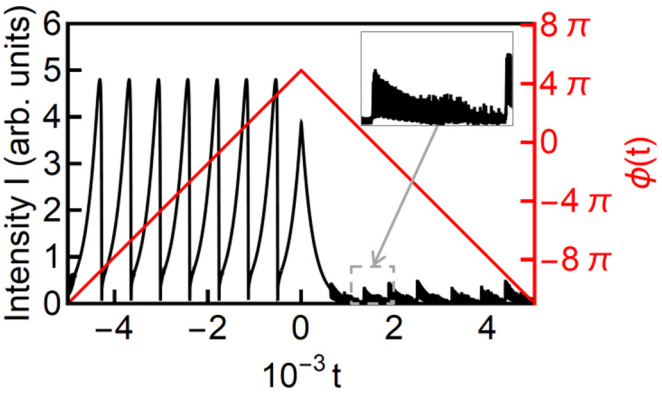

FIG. 2. Numerical simulation of the model equations (3)–(4) displaying mode-hopping events in the positive sweep direction. The frequency sweeping in the negative direction exhibits chaotic dynamics. The zero point on the x axis is the turning point of the sweep, and the sweeping function $\phi(t)$ is shown (in red) above the intensity. The parameters are $\eta = 1$, $\gamma = 0.25$, $\varepsilon = 0.01$. The other parameter values are the same as in Fig. 1.

to a fold bifurcation from a cavity mode that is responsible for the mode-hopping sequence as we progressively increase ϕ_0. The mode-hopping sequence forms large-amplitude bursts which are similar the to neuromorphic design of square-wave bursting oscillations [22].

Formation of the large-amplitude burst is detailed in Fig. 3 where the bifurcation diagram of the steady-state and periodic solutions is shown together with the long-time solution of

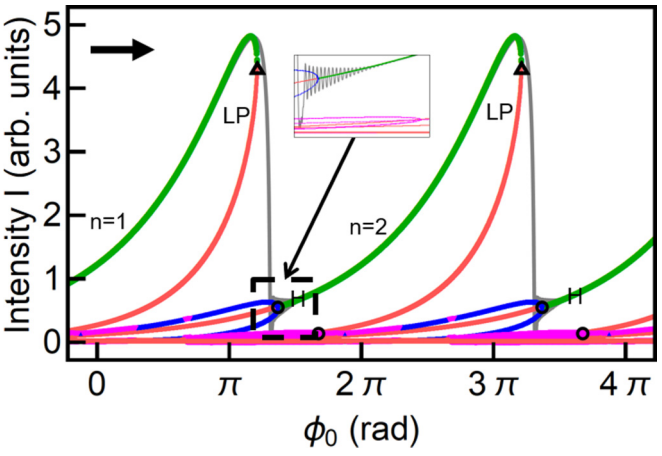

FIG. 3. The power-dropout and power-recovery large-amplitude cycle (dark gray) in the plane (I, ϕ_0) is shown together with the bifurcation diagram of the cavity modes $n = 1$ and $n = 2$ in the interval $0 < \phi_0 < 4\pi$. Green (red) lines correspond to the stable (unstable) steady-state solutions. Blue (magenta) lines correspond to the stable (unstable) periodic solutions. Circles and triangles mark an Andronov-Hopf bifurcation point and a fold bifurcation, respectively. The figure shows that the power-dropout and power-recovery cycle follows a stable branch of periodic solutions until it reaches a supercritical Andronov-Hopf bifurcation point H, then follows the stable steady-state branch until it reaches a fold bifurcation point LP. The black arrow indicates the direction of sweep. The values of the fixed parameters are the same as in Fig. 2.

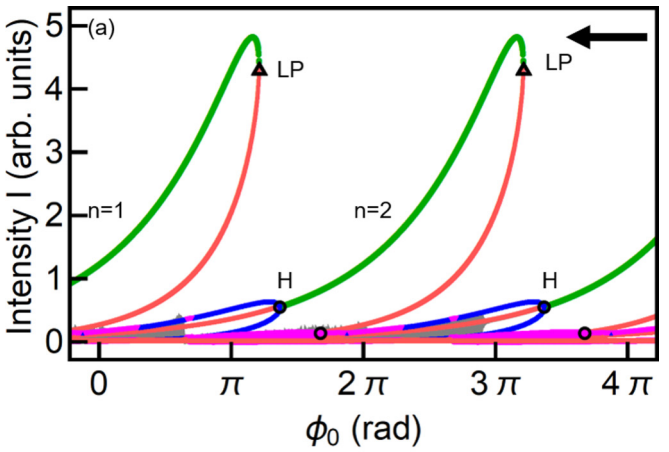

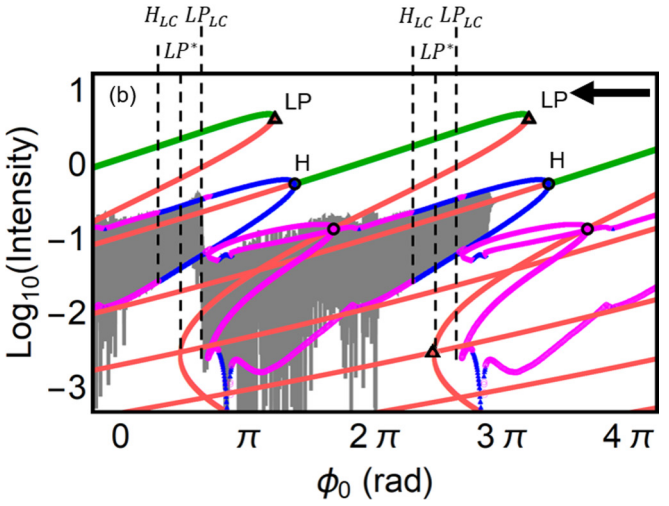

FIG. 4. Dynamical evolution of the intensity with sweeping frequency in the positive direction (dark gray) in the plane (I, ϕ_0) is shown together with the bifurcation diagram in linear (a) and logarithmic scales (b). The figure shows that the branch of periodic solutions (dark gray) is emerging from supercritical Andronov-Hopf bifurcation point H, follows a stable branch of periodic solutions, undergoes a secondary Hopf bifurcation H_{LC}, and develops into chaos with various stability changes until it reaches a limit point of limit cycles LP_{LC} from where it jumps back to the vicinity of the Andronov-Hopf bifurcation. The black arrow indicates the direction of sweep. LP^* is the CW solution fold bifurcation point at low-intensity value. The coloring, the marks, and the fixed parameters are the same as in Fig. 3.

Eqs. (3)–(4) (in dark gray) for the positive frequency sweep direction relative to the filter profile $\phi(t) = \varepsilon t$, $\varepsilon = 0.01$. The single-mode steady state changes stability at the point H with the increase of ϕ_0, and the branch of stable periodic solutions emerges from the supercritical Andronov-Hopf bifurcation point at the relaxation oscillation frequency. LP marks a limit point of steady states at which the power dropout happens. The laser follows the steady-state branch $n = 1$ as ϕ_0 increases until it passes LP and then drops down to sustained oscillations of the lower branch of periodic solutions at $n = 2$ and returns to the steady-state branch passing the Andronov-Hopf bifurcation H. As is visible in Fig. 3, the Andronov-Hopf

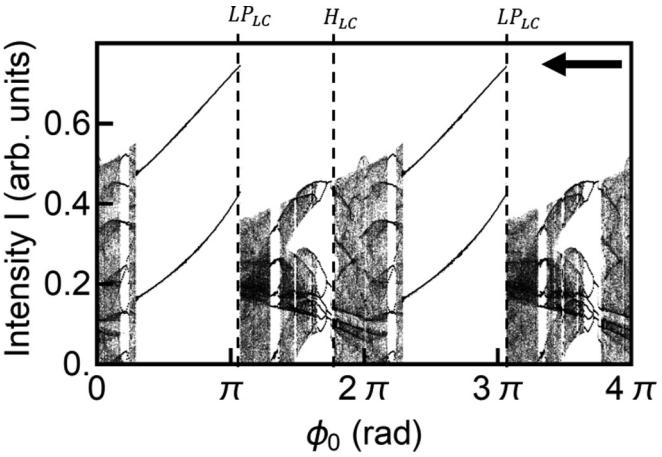

FIG. 5. Time-average extrema of $I(t)$ obtained numerically for the negative direction of the frequency sweep for low-amplitude bursting. The black arrow indicates the direction of sweep. The fixed parameters and the marks are the same as in Fig. 4.

bifurcation transition to steady state can be delayed in the absence of noise [23].

Let us now follow a low-amplitude bursting cycle which appears at the branch $n = 2$ after a supercritical Andronov-Hopf bifurcation H for the negative sweep direction $\phi(t) = -\varepsilon t$, $\varepsilon = 0.01$. It is shown in dark gray in Fig. 4. After the transition to the stable periodic oscillations the laser follows the branch $n = 2$ of limit-cycle oscillations as ϕ_0 decreases until it reaches LP_{LC}. The laser then jumps up to the upper branch $n = 1$, starting a new bursting cycle. The jump up may happen slightly before LP_{LC}. The folding point of the Andronov-Hopf bifurcation branch, which we denote by LP_{LC} in Fig. 4(b), is important for the formation of the low-amplitude bursting. This point corresponds to a saddle-node bifurcation of limit cycles below which neither stable nor unstable periodic oscillations are possible. Different dynamics between H and LP_{LC} can be seen in Fig. 5, which shows the extrema of the oscillations as we progressively decrease ϕ_0 from H. After a secondary Hopf bifurcation H_{LC}, quasiperiodicity, and weak chaos, the laser jumps up to the higher branch. The response of the laser to the slowly sweeping narrow band filtering thus takes the form of low-amplitude bursts of spiking.

IV. CONCLUSION

In this paper, we have considered a delay differential equation model for a laser with an intracavity swept filter, and theoretically analyzed the bifurcation structure of a short-cavity swept source. Unlike the long-cavity devices, the continuous wave solution of the model equations is strongly asymmetric with a foldover similar to nonlinear resonance curve with hysteresis [19,20]. The foldover allows coexistence of single-mode branches, which changes the character of the mode hopping compared to long-cavity devices. Additionally, the foldover defines two bursting phenomena which form sufficiently different laser outputs depending on the sweep direction. Such a behavior is similar to that observed in other swept sources; for this reason the increasing wavelength sweep will lead to more coherent output but with mode hops, while the decreasing wavelength sweep will lead to a continuous sweep with a lower coherence length as for other swept sources [16,18].

ACKNOWLEDGMENTS

A.V.K., P.S.D., and E.A.V. acknowledge the Government of the Russian Federation (Grant 08-08). A.V.K., P.S.D., G.H., and E.A.V. acknowledge the support of H2020-MSCA-RISE-2018 HALT. The work of A.V.K. and E.A.V. was supported by the Ministry of Education and Science of the Russian Federation (Passport No. 2019-1442). A.P. and A.G.V. acknowledge the support by the subproject B5 of the DFG Collaborative Research Center SFB 787. A.P. is funded by the DFG under Germany's Excellence Strategy—The Berlin Mathematics Research Center MATH+ (EXC-2046/1, Project ID: 390685689).

[1] W. Drexler and J. G. Fujimoto (eds.), *Optical Coherence Tomography* (Springer, Berlin, 2008).
[2] S. R. Chinn, E. A. Swanson, and J. G. Fujimoto, Opt. Lett. **22**, 340 (1997).
[3] D. C. Adler, W. Wieser, F. Trepanier, J. M. Schmitt, and R. A. Huber, Opt. Express **19**, 20930 (2011).
[4] W. Atia, M. Kuznetsov, and D. Flanders, US Patent Publication No. US 2009/0059971 A1 (2009).
[5] B. Johnson and D. Flanders, US Patent No. US 10,371,499 B2 (2019).
[6] B. Johnson, W. Atia, M. Kuznetsov, B. D. Goldberg, P. Whitney, and D. C. Flanders, Biomed. Opt. Express **8**, 1045 (2017).
[7] B. Johnson, W. Atia, M. Kuznetsov, B. D. Goldberg, P. Whitney, and D. C. Flanders, Opt. Express **26**, 34909 (2018).
[8] V. Jayaraman, G. Cole, M. Robertson, A. Uddin, and A. Cable, Electron. Lett. **48**, 867 (2012).
[9] T. P. Butler, S. Slepneva, P. M. McNamara, K. Neuhaus, D. Goulding, M. Leahy, and G. Huyet, IEEE Photonics J. **9**, 1 (2017).
[10] S. Moon and E. S. Choi, Biomed. Opt. Express **8**, 1110 (2017).
[11] T. P. Butler, D. Goulding, S. Slepneva, B. O'Shaughnessy, S. P. Hegarty, G. Huyet, and B. Kelleher, Opt. Express **27**, 7307 (2019).
[12] M. Bonesi, M. P. Minneman, J. Ensher, B. Zabihian, H. Sattmann, P. Boschert, E. Hoover, R. A. Leitgeb, M. Crawford, and W. Drexler, Opt. Express **22**, 2632 (2014).
[13] R. Pajković, Y. Tian, S. Latkowski, K. A. Williams, and E. A. M. Bente, in *Novel In-Plane Semiconductor Lasers XVIII*, edited by A. A. Belyanin and P. M. Smowton (SPIE, Bellingham, 2019), Vol. 10939, p. 1093912.
[14] C. Jirauschek, B. Biedermann, and R. Huber, Opt. Express **17**, 24013 (2009).
[15] E. A. Avrutin and L. Zhang, Eur. Phys. J. B **92**, 137 (2019).

[16] S. Slepneva, B. Kelleher, B. O'Shaughnessy, S. Hegarty, A. Vladimirov, and G. Huyet, Opt. Express **21**, 19240 (2013).
[17] A. G. Vladimirov and D. Turaev, Phys. Rev. A **72**, 033808 (2005).
[18] S. Slepneva, B. O'Shaughnessy, B. Kelleher, S. Hegarty, A. Vladimirov, H.-C. Lyu, K. Karnowski, M. Wojtkowski, and G. Huyet, Opt. Express **22**, 18177 (2014).
[19] K. Otsuka and S. Kobayashi, Electron. Lett. **19**, 262 (1983).
[20] S. Coen and M. Erkintalo, Opt. Lett. **38**, 1790 (2013).
[21] K. Engelborghs, T. Luzyanina, and D. Roose, ACM Trans. Math. Softw. **28**, 1 (2002).
[22] E. M. Izhikevich, *Dynamical Systems in Neuroscience* (MIT Press, Cambridge, MA, 2010).
[23] S. M. Baer, T. Erneux, and J. Rinzel, SIAM J. Appl. Math. **49**, 55 (1989).